Organic Geochemistry 103 (2017) 51–62

Contents lists available at ScienceDirect

Organic Geochemistry

journal homepage: www.elsevier.com/locate/orggeochem

Hydrocarbon gas generation from pyrolysis of extracts and residues of low maturity solid bitumens from the Sichuan Basin, China

Zixiang Wang [a,b,c], Yongli Wang [a,*], Baoxiang Wu [a], Gen Wang [a,b], Zepeng Sun [a,b], Liang Xu [a,b], Shenzheng Zhu [a,b], Lina Sun [a,b], Zhifu Wei [a]

[a] Key Laboratory of Petroleum Resources, Gansu Province/Key Laboratory of Petroleum Resources Research, Institute of Geology and Geophysics, Chinese Academy of Sciences, Lanzhou 730000, China
[b] University of Chinese Academy of Sciences, Beijing 100049, China
[c] Sinopec Jianghan Oilfield Company, Wuhan, Hubei 430223, China

ARTICLE INFO

Article history:
Received 11 November 2015
Received in revised form 14 October 2016
Accepted 14 October 2016
Available online 19 October 2016

Keywords:
Hydrocarbon gas generation
Sinian-Cambrian
Bitumen "A"
Insoluble residual
Stable carbon isotope
Kinetics

ABSTRACT

Two sets of pyrolysis experiments were performed on bitumen "A" (BA) and extracted organic matter (ER) from low-maturity solid bitumen at heating rates of 2 °C/h and 20 °C/h in confined systems (gold capsules). The main observations can be listed as follows: (1) BA and ER have high generation potential of hydrocarbons and were a significant secondary hydrocarbon source. (2) Both have similar evolutionary characteristics of hydrocarbon gas generation, and have high C_1/C_{1-5} values than those from an Ordovician normal oil. Ea distributions of the methane generated from pyrolysis of BA and ER is far lower than that of Ordovician normal oil. (3) The evolution of stable carbon isotope values of individual hydrocarbon gases can be divided into three stages. Plots of $\ln C_1/C_2$ versus $\ln C_2/C_3$, $\delta^{13}C_1-\delta^{13}C_2$ versus $\ln(C_1/C_2)$ and $\delta^{13}C_2-\delta^{13}C_3$ versus $\ln(C_2/C_3)$ clearly illustrate the characteristics of hydrocarbon gases generated from BA and ER at different thermal maturity stages. (4) Basin modelling reconstructions of the hydrocarbon generation history of BA and ER in Sinian and Cambrian strata respectively indicate: Hydrocarbon gases generation from ER started in the Middle Jurassic, and ended in the Early Cretaceous with a maturity equivalent to Easy%Ro ≈ 2.2%. The final conversion rate of C_{1-5} and C_1 are 0.71 and 0.48, respectively. Hydrocarbon gas generation from BA started in the Early Jurassic, and ended in the Early Cretaceous with an Easy%Ro ≈ 3.0%. The final conversion rate of C_{1-5} and C_1 are 0.90 and 0.81, respectively.

1. Introduction

Interest in Sinian-lower Palaeozoic petroleum systems in the Sichuan Basin has increased during the last decade (Zou et al., 2014). Since 2011, giant gas fields with estimated reserves of more than one trillion cubic meters have been discovered in Sinian and Cambrian strata in the Gaoshiti-Moxi region, central Sichuan paleo-uplift (Du et al., 2014).

There is still significant debate ongoing regarding the source of the Sinian-Cambrian gas accumulations, and the history and characteristics of hydrocarbon gas generation. Abundant pyrobitumen deposits have been found in Sinian to Mesozoic reservoir rocks in the Tarim Basin, Sichuan Basin, and other areas in southern China (Xie et al., 2005; Zhang et al., 2005; Wei et al., 2007; Xiao et al., 2007; Jin et al., 2014). The pyrobitumen is interpreted to be derived from crude oils that have undergone intense thermal degradation and to be evidence of a secondary oil cracking origin for the gas in Sinian-Cambrian gas fields. Many studies have focused on high-maturity pyrobitumen (Xie et al., 2005; Zhang et al., 2005; Wei et al., 2007; Xiao et al., 2007; Jin et al., 2014), but few have reported on the hydrocarbon gas generation characteristics, kinetics and history of Sinian-Cambrian source rocks because of a lack of suitable low-maturity source rocks (Wang et al., 2013). Fortunately, abundant low-maturity solid bitumen has been discovered in the NE part of the Longmenshan fold-thrust belt in the NW Sichuan Basin. A popular idea is that the low-maturity bitumen originated from the Lower Cambrian, which has been proposed as the major source rock of Sinian-Cambrian gas accumulations (Zhou et al., 2007, 2013; Deng et al., 2008; Huang and Wang, 2008; Liu et al., 2009).

In this study, bitumen "A" (BA) and extraction residue (ER) were obtained from a low-maturity bitumen sample and pyrolyzed in sealed gold tube experiments over a range of temperatures. The gas composition, hydrocarbon gas stable carbon isotope signatures and the pertinent evolution history of hydrocarbon gases from BA

* Corresponding author. Fax: +86 931 4960828.
E-mail address: wyll6800@lzb.ac.cn (Y. Wang).

http://dx.doi.org/10.1016/j.orggeochem.2016.10.011
0146-6380/

and ER were assessed with the intent of providing new insights into the origin of gas in the Sinian-Cambrian reservoirs in the Sichuan Basin.

2. Samples and experimental methods

2.1. Samples

A sample of solid bitumen was collected from an outcrop in Kuangshanliang, northwest Sichuan Basin. The outcrop is located in an exhumed paleo-reservoir. Previous studies indicate that the solid bitumen was derived from crude oil, charged from Lower Cambrian black shales during the Early-mid Jurassic and has not suffered significant thermal degradation due to post-Jurassic uplift of the reservoir rock (Zhou et al., 2013; Zhang et al., 2014). The solid bitumens are depleted in low molecular weight hydrocarbons due to evaporation and biodegradation during exposure to the atmosphere (Huang and Wang, 2008) (Fig. 1). Geochemical data for the solid bitumen are presented in Table 1.

2.1.1. Sample preparation

An aliquot of the bituminous dike sample was crushed into powder and extracted for 72 h with chloroform using a Soxhlet apparatus. Chloroform soluble bitumen (Bitumen "A", BA) and residue (Extracted residual, ER) were obtained with relative proportions of 8.3:91.7 (v:v) respectively. SARA analysis and stable carbon isotope data of BA and ER are presented in Table 2.

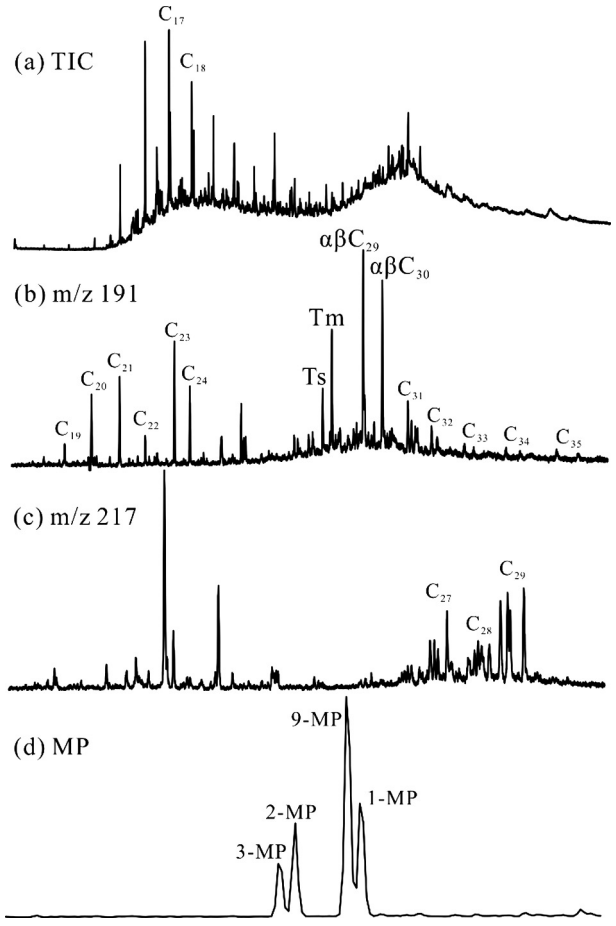

Fig. 1. (a) GC–MS total ion chromatograms (TIC) of the saturated fraction in EOM of bitumen; (b) *m/z* 191 mass chromatograms, displaying terpane distribution; (c) *m/z* 217 mass chromatograms, displaying sterane distribution; and (d) *m/z* 192 mass chromatograms, displaying methylphenanthrenes distribution.

2.2. Confined pyrolysis experiments

Two sets of pyrolysis experiments were conducted, on BA and ER samples respectively using flexible gold capsules (4 mm outside diameter, 0.25 mm wall thickness and 40-mm length) and pyrolyzed within steel pressure vessels.

The capsules were welded at one end before loading samples. Each capsule was loaded with 15–60 mg sample. For samples heated at low temperature, a larger amount of sample was used to produce sufficient gas for subsequent compositional analyses. Once loaded, the capsule was purged with argon, before the open end was squeezed with a vice to create an initial seal and then welded in the presence of argon. During welding, the previously welded end of gold tube was submerged in cold water to minimize heat transferred to the reactants.

The pyrolysis system can accommodate 16 pressure vessels in a single furnace. A fan was installed at the bottom of the furnace to ensure a homogeneous temperature inside. The vessels were previously filled with water and two capsules containing BA and ER were placed together in each vessel. The internal pressure of the vessels, which were connected to each other via tubes, was adjusted to 50 MPa by pumping water into the vessels before heating. This pressure setting was used to simulate subsurface pressure conditions while also taking experimental safety into account. This pressure was maintained automatically by pumping water into or out of the vessels during the pyrolysis experiments. The range of error of the pressure is < ± 0.1 MPa.

The vessels were pre-heated from room temperature (about 20 °C) to 250 °C within 10 h and then from 250 °C to 600 °C at a rate of 20 °C/h or 2 °C/h. Two thermocouples were used to monitor the temperature during the pyrolysis. One thermocouple was attached to the outside wall of a vessel to monitor the oven temperatures while the other was placed inside the same vessel to monitor the temperature inside. The former temperatures were slightly higher than the latter with a difference < 0.5 °C. The range of error of the recorded temperature was < ± 1 °C. The vessel with two gold tube sample (BA and ER) was removed from the oven at temperature intervals of 12 °C or 24 °C from 336 °C to 600 °C. Each vessel was quenched to room temperature in cold water within 10 min. The thermal maturity of samples in the simulation experiment was calculated as the vitrinite reflectance equivalence using the 'Easy%Ro' method of Sweeney and Burnham (1990).

2.3. Chemical and carbon isotopic analyses of gas components

After pyrolysis, the volatile components in the capsules were collected in a special device connected to an Agilent 6890N gas chromatograph (GC) modified by Wasson ECE Instrumentation, as described previously by Pan et al. (2006, 2008). Briefly, the whole device was first evacuated by a vacuum pump to reach an internal pressure < 1×10^2 Pa. The gold capsule was then pierced in the vacuum device with a needle, allowing the gases to escape into the device. The valve connecting the device and the modified GC was opened to allow the gas components to enter the GC, through which the GC analyses of both the organic and inorganic gas components were performed in an automatically controlled procedure. GC analyses were conducted with a two-channel Hewlett–Packard 6890 GC custom configured (Wassen ECE) with eight (two capillary and six packed) columns and one FID and two TCD providing simultaneous detection of several organic and inorganic gases. Helium (for inorganic gas analysis) or nitrogen (organic) were used as carrier gases and the GC oven was programmed from 70 °C (held for 5 min) to 130 °C at 15 °C/min, then to a final 180 °C at 25 °C/min (held for 4 min). The analysis of all gases was carried out by one single injection.

Table 1
Geochemical characteristics of the bitumen sample used in the pyrolysis experiments.

Sample	TOC (%)	S_1 (mg/g)	S_2 (mg/g)	S_3 (mg/g)	HI (mg/g)	T_{max} (°C)	$\delta^{13}C$ (‰)	Ts/Tm	MPI-1	MPI-2
Solid bitumen	58.0	2.42	36.96	0.40	637.06	401	−35.3	0.52	0.47	0.57

Table 2
Gross compositions and stable isotope values for BA, ER and Ordovician oil used in the pyrolysis experiments.

Sample	Saturate (%)	Aromatics (%)	Resins (%)	Asphaltenes (%)	$\delta^{13}C$ (‰)
BA (8.3%)	0.04	1.15	14.90	83.90	−35.8
ER (91.7%)	–	–	–	–	−35.2
Ordovician oil[a]	81.7	7.0	5.9	5.4	−32.4

[a] Data are from Pan et al. (2010).

After GC analysis, the remaining gas within the device, approximately 80% of the initial volume, was sampled for isotopic composition analysis using a syringe through the septum on the device. Isotope analysis was performed on a VG Isochrom II isotope ratio mass spectrometer (IRMS) interfaced with an HP 5890 GC, fitted with a Poraplot Q column (30 m × 0.32 mm i.d.). Helium was used as the carrier gas. The column head pressure was 8.5 psi. The GC oven temperature was initially held at 40 °C for 3 min, ramped from 40 °C to 180 °C at 20 °C/min, and held at 180 °C for 5 min. Carbon isotope ratios for individual gaseous hydrocarbon compounds were measured using CO_2 as a reference gas, which was automatically introduced into the IRMS at the beginning and end of each analysis. The carbon isotope value of the CO_2 reference gas was calibrated against NBS-22 oil. In addition, a standard mixture of gaseous hydrocarbons (C_1–C_4), with known isotope compositions calibrated by our laboratory, was used daily to check the performance of the instrument. The standard deviation for replicate analyses of this mixture is < 0.3‰ for each compound.

2.4. Kinetic modelling of the generation of hydrocarbon gases

Kinetic parameters were determined for the generation of gaseous hydrocarbons using the Kinetics 2000 software developed by Braun and Burnham (1998). We set a fixed *A* factor of $1 \times 10^{14}\ S^{-1}$ for the generation of methane in volume, and a fixed *A* factor of $1 \times 10^{15}\ S^{-1}$ for the generation of C_{1-5} in volume, following the approach of previous studies (Pan et al., 2010, 2012). The Kinetics 2000 software generates the value of the *A* factor and the discrete distribution of activation energies based on the input data from the two heating rates (i.e., time, temperature and the conversion value for C_1 and C_{1-5} generation).

3. Results and discussion

3.1. Yields of gas components

The amounts and ratios of gas components produced by pyrolysis of BA and ER are shown in Table 3 and Fig. 2. For both two sets of experiments, the yield of methane increased consistently with higher experimental temperatures. For BA, the final yield of methane generated was 352.02 ml/g at the 20 °C/h heating rate and 364.15 ml/g at the 2 °C/h heating rate. For ER, the final amount of methane generated is 268.90 ml/g at the 20 °C/h heating rate and 271.35 ml/g at the 2 °C/h heating rate. Under the same temperature conditions, the yields of methane generated from ER were lower than those from BA (Fig. 2a).

For the two sets of experiments with BA and ER, the yields of ethane, propane, butane and pentane generated initially increased with temperature, then decreased with further temperature increase, peaking at their respective critical temperatures (CT). Under the same temperature conditions, the amounts of wet gas generated from ER was lower than those from BA.

For the two sets of experiments with BA and ER, the volume yields of the C_{1-5} increased with temperature over the whole temperature range (Fig. 2f, Table 3). Overall, the yield of C_{1-5} generated was greater from BA than from ER. For example, in the 20 °C/h heating rate experiment, the maximum volume and mass yields of the C_{1-5} from BA were 360.23 ml/g and 266.82 mg/g, respectively; whereas from ER the yields were only 273.36 ml/g and 205.54 mg/g, respectively (Fig. 2f).

3.2. Ratios of C_1/C_{1-5}

For both experiments with BA and ER, the C_1/C_{1-5} ratio first decreased as temperature increased from 334.7 to 407.2 °C, then increased as temperature increased further in the 20 °C/h heating rate experiment. For 2 °C/h heating rate experiment, this ratio first decreased from 335.0 °C to 359.1 °C and then increased as temperature increased further (Fig. 3). The C_1/C_{1-5} values were similar for both sets of experiments with BA and ER, and were significantly higher than those from pyrolysis of Ordovician oil (composed primarily of saturates) in the studies by Pan et al. (2010, 2012) (Table 2). Compared with the Ordovician oil used by Pan et al. (2010, 2012), which is composed primarily of saturates, BA mainly consists of asphaltenes (83.9%) and resins (14.9%). This suggests that asphaltenes and resins are more prone to produce primarily methane, while saturates are more likely to produce wet gases. This interpretation is consistent with the results of previous studies (Tian et al., 2012).

3.3. Stable carbon isotope compositions of gas components

The $\delta^{13}C$ profiles of methane, ethane and propane of both the 20 °C/h and the 2 °C/h pyrolysis series are shown in Fig. 4. The carbon isotope compositions of methane, ethane and propane respectively were similar for both the two sets of experiments with BA and ER. The evolution of stable carbon isotope values of individual hydrocarbon gas could be divided into three stages in our experiments: (1) When %Ro < 0.8%, $\delta^{13}C_1$, $\delta^{13}C_2$ and $\delta^{13}C_3$ all become isotopically lighter with maturity, and show a partial carbon isotope trend reversals where $\delta^{13}C_2 > \delta^{13}C_3 > \delta^{13}C_1$. The $\delta^{13}C_2$ and $\delta^{13}C_3$ values are more positive than the carbon isotope values of the initial samples, and the gap between $\delta^{13}C_2$ and $\delta^{13}C_3$ narrows as maturity increases. Similar results were observed in pyrolysis experiment of asphaltenes by Wang et al. (2010). This is quite different from kerogen or oil cracking that generally is characterized by normal isotope ordering, i.e., $\delta^{13}C_1 < \delta^{13}C_2 < \delta^{13}C_3$. The reason for the isotope reversal is still not fully understood and needs further research on reaction mechanisms. (2) In the %Ro range from 0.8% to 1.6%, the changes in $\delta^{13}C_1$, $\delta^{13}C_2$ and $\delta^{13}C_3$ are not

Table 3
Hydrocarbon yields and their stable carbon isotope compositions from the pyrolysis experiments of BA and ER.

T (°C)	EasyRo (%)	C_1 (ml/g)	C_2 (ml/g)	C_3 (ml/g)	$C_4 + C_5$ (ml/g)	C_{2-5} (ml/g)	C_{1-5} (ml/g)	C_1 (mg/g)	C_2 (mg/g)	C_3 (mg/g)	$C_4 + C_5$ (mg/g)	C_{2-5} (mg/g)	C_{1-5} (mg/g)	C_1/C_{1-5}[a] (%)	δC_1 (‰)	δC_2 (‰)	δC_3 (‰)
Bitumen "A" (20 °C/h)																	
334.7	0.6	0.79	0.36	0.16	0.03	0.55	1.34	0.57	0.49	0.31	0.09	0.88	1.45	39.05	−46.3	−24.3	−32.1
358.9	0.7	2.06	1.03	0.62	0.25	1.90	3.96	1.47	1.38	1.22	0.69	3.28	4.75	30.91	−46.7	−28.6	−33.2
383.2	0.8	6.56	3.22	2.48	2.04	7.73	14.29	4.68	4.31	4.87	5.53	14.71	19.39	24.15	−48.0	−34.9	−36.2
407.2	1.0	18.82	10.28	7.02	5.64	22.94	41.76	13.44	13.76	13.79	15.32	42.87	56.31	23.87	−51.1	−37.6	−36.4
431.1	1.2	38.38	18.86	13.14	10.43	42.43	80.81	27.42	25.26	25.81	28.31	79.38	106.80	25.67	−51.0	−37.9	−36.8
455.2	1.5	67.62	31.99	23.76	19.82	75.56	143.18	48.30	42.84	46.66	53.79	143.30	191.59	25.21	−48.6	−39.0	−36.1
479.1	1.8	108.37	46.52	31.10	17.71	95.34	203.70	77.41	62.30	61.09	48.08	171.48	248.88	31.10	−46.7	−37.2	−33.0
503.0	2.2	151.26	53.47	28.07	7.92	89.46	240.72	108.04	71.61	55.14	21.49	148.24	256.29	42.16	−43.7	−32.3	−25.1
527.2	2.6	220.97	55.67	14.95	1.86	72.49	293.46	157.84	74.56	29.37	5.05	108.99	266.82	59.15	−43.1	−30.9	−18.5
551.3	3.1	273.74	45.02	4.43	0.31	49.75	323.49	195.53	60.29	8.70	0.83	69.82	265.35	73.69	−42.7	−25.9	–
575.4	3.5	322.83	24.25	0.52	0.03	24.80	347.63	230.59	32.48	1.02	0.08	33.58	264.17	87.29	−40.7	−16.6	–
599.7	3.9	352.02	8.09	0.11	0.00	8.21	360.23	251.45	10.84	0.22	0.01	11.07	262.51	95.78	−38.7	−11.5	–
Bitumen "A" (2 °C/h)																	
335.0	0.7	3.34	1.79	1.17	0.55	3.51	6.85	2.39	2.40	2.30	1.50	6.19	8.58	27.83	−50.4	−33.6	−35.7
359.1	0.9	9.56	5.58	4.28	3.76	13.63	23.19	6.83	7.48	8.41	10.21	26.10	32.93	20.74	−50.0	−36.9	−36.1
383.3	1.1	23.22	12.19	8.59	8.13	28.91	52.13	16.59	16.32	16.87	22.07	55.26	71.85	23.09	−49.4	−37.3	−36.7
407.4	1.4	48.43	22.02	14.87	12.13	49.02	97.46	34.60	29.50	29.22	32.91	91.62	126.22	27.41	−50.8	−38.3	−36.5
431.5	1.7	85.36	35.75	24.08	16.44	76.27	161.63	60.97	47.88	47.30	44.62	139.80	200.77	30.37	−47.1	−37.7	−35.2
455.5	2.1	141.86	50.44	28.28	10.87	89.59	231.45	101.33	67.55	55.56	29.50	152.61	253.93	39.90	−44.3	−35.8	−30.8
479.6	2.5	204.09	53.21	18.69	3.44	75.34	279.43	145.78	71.26	36.71	9.35	117.32	263.10	55.41	−43.3	−31.4	−23.0
503.7	3.0	274.98	39.39	4.45	0.32	44.17	319.15	196.42	52.76	8.74	0.87	62.37	258.79	75.90	−41.3	−25.7	−5.2
527.3	3.4	324.12	18.20	0.37	0.02	18.59	342.71	231.52	24.37	0.73	0.04	25.15	256.66	90.20	−39.5	−16.3	–
551.5	3.9	353.05	4.21	0.06	0.00	4.27	357.32	252.18	5.64	0.12	0.01	5.77	257.94	97.76	−39.0	–	–
575.5	4.2	358.73	1.75	0.03	0.00	1.78	360.51	256.24	2.35	0.05	0.00	2.40	258.64	99.07	−37.9	–	–
599.3	4.4	364.15	1.70	0.02	0.00	1.72	365.87	260.11	2.28	0.04	0.00	2.31	262.42	99.12	−37.7	–	–
Extracted residual (20 °C/h)																	
334.7	0.6	0.50	0.23	0.12	0.02	0.36	0.86	0.35	0.31	0.23	0.05	0.58	0.94	37.79	−45.5	−25.7	−32.4
358.9	0.7	1.55	0.79	0.50	0.17	1.45	3.00	1.11	1.06	0.97	0.45	2.48	3.59	30.86	−46.5	−30.2	−32.6
383.2	0.8	5.55	3.13	1.97	1.12	6.22	11.77	3.96	4.19	3.88	3.03	11.10	15.06	26.31	−49.4	−36.3	−35.4
407.2	1.0	14.02	8.01	5.71	5.51	19.22	33.24	10.01	10.72	11.22	14.95	36.88	46.90	21.35	−48.6	−37.2	−37.1
431.1	1.2	27.68	14.28	10.34	10.09	34.71	62.39	19.77	19.12	20.31	27.40	66.83	86.60	22.83	−47.8	−36.8	−36.2
455.2	1.5	53.22	24.75	18.01	15.56	58.32	111.54	38.01	33.15	35.38	42.23	110.76	148.77	25.55	−47.9	−37.9	−35.6
479.1	1.8	89.31	36.05	21.85	10.10	68.00	157.31	63.79	48.29	42.91	27.42	118.62	182.41	34.97	−45.9	−35.9	−33.4
503.0	2.2	125.48	42.39	19.99	5.35	67.73	193.21	89.63	56.77	39.26	14.52	110.55	200.18	44.77	−44.8	−34.7	−26.3
527.2	2.6	172.32	38.15	7.58	0.81	46.53	218.85	123.09	51.09	14.88	2.19	68.16	191.25	64.36	−44.6	−30.4	−16.3
551.3	3.1	220.54	31.61	2.66	0.17	34.43	254.98	157.53	42.33	5.22	0.46	48.01	205.54	76.64	−41.3	−26.5	–
575.4	3.5	258.45	14.71	0.19	0.01	14.91	273.36	184.61	19.70	0.38	0.03	20.11	204.71	90.18	−40.5	−19.2	–
599.7	3.9	268.90	4.29	0.06	0.00	4.36	273.26	192.07	5.75	0.12	0.01	5.88	197.95	97.03	−38.3	−13.8	–
Extracted residual (20 °C/h)																	
335.0	0.7	2.51	1.32	0.81	0.33	2.47	4.98	1.79	1.77	1.59	0.91	4.27	6.06	29.59	−48.6	−34.0	−34.5
359.1	0.9	7.40	4.54	3.14	2.29	9.97	17.37	5.29	6.08	6.17	6.21	18.46	23.75	22.26	−50.8	−37.9	−36.6
383.3	1.1	19.32	10.53	6.56	4.71	21.80	41.12	13.80	14.10	12.89	12.79	39.78	53.58	25.75	−50.9	−37.0	−36.8
407.4	1.4	37.56	17.95	12.42	11.07	41.44	78.99	26.83	24.03	24.39	30.06	78.48	105.30	25.47	−47.9	−37.3	−36.5
431.5	1.7	68.23	28.63	18.78	12.62	60.03	128.26	48.73	38.34	36.89	34.25	109.49	158.22	30.80	−47.0	−37.2	−34.7
455.5	2.1	112.35	38.34	20.50	8.10	66.94	179.29	80.25	51.35	40.27	21.98	113.60	193.85	41.40	−44.7	−34.7	−29.9
479.6	2.5	160.19	39.34	12.48	2.08	53.89	214.09	114.42	52.69	24.51	5.63	82.83	197.26	58.01	−43.3	−31.3	−21.7
503.7	3.0	212.12	28.68	2.18	0.14	31.01	243.12	151.51	38.41	4.29	0.38	43.08	194.60	77.86	−42.0	−25.8	−6.5
527.3	3.4	251.06	11.59	0.20	0.01	11.79	262.85	179.33	15.52	0.38	0.02	15.93	195.26	91.84	−40.1	−17.6	–
551.5	3.9	263.69	1.91	0.03	0.00	1.94	265.63	188.35	2.56	0.06	0.00	2.62	190.97	98.63	−38.8	–	–
575.5	4.2	267.59	1.00	0.01	0.00	1.01	268.60	191.13	1.34	0.02	0.00	1.36	192.50	99.29	−37.7	–	–
599.3	4.4	271.35	0.82	0.01	0.00	0.83	272.18	193.82	1.10	0.02	0.00	1.12	194.94	99.43	−37.5	–	–

[a] Calculated based on weight yields of hydrocarbon gases.

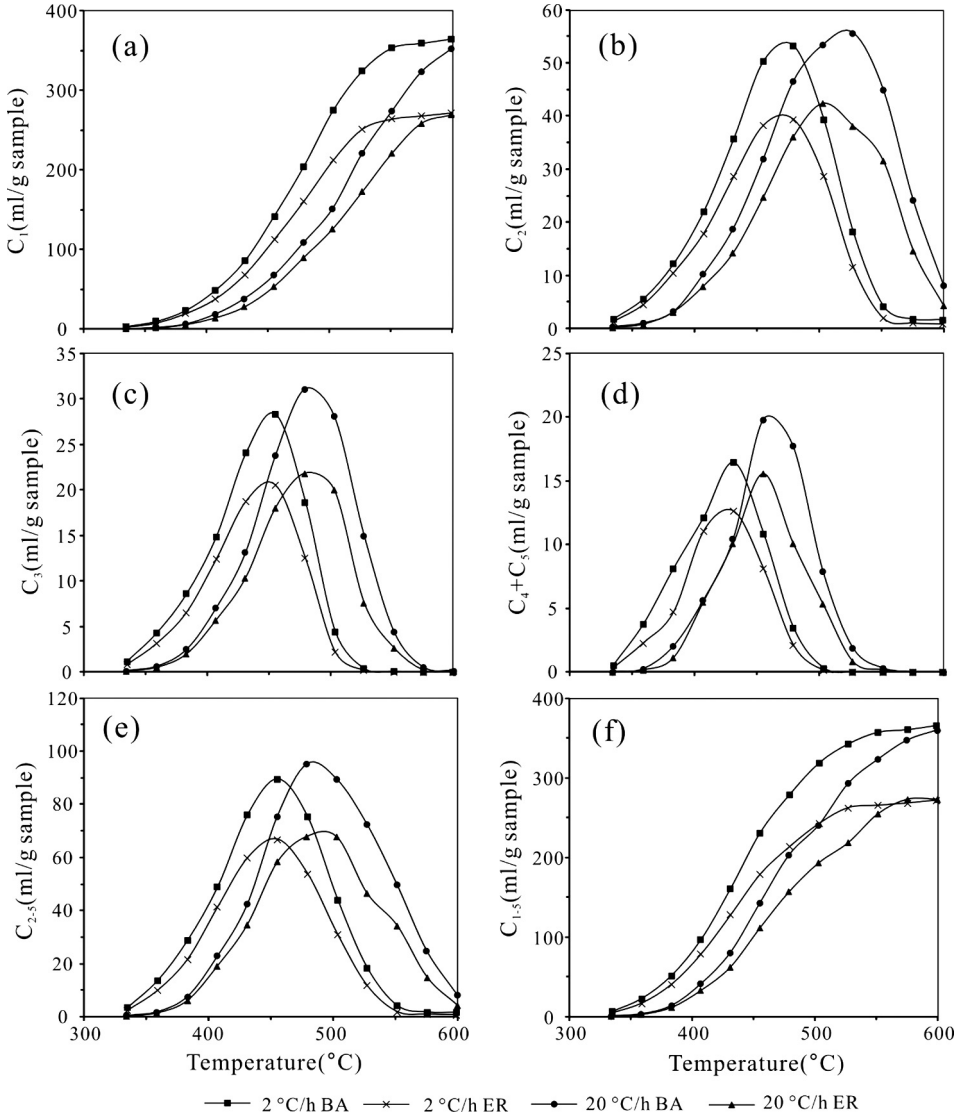

Fig. 2. Yields of gaseous hydrocarbons versus temperature for BA and ER at the two heating temperatures.

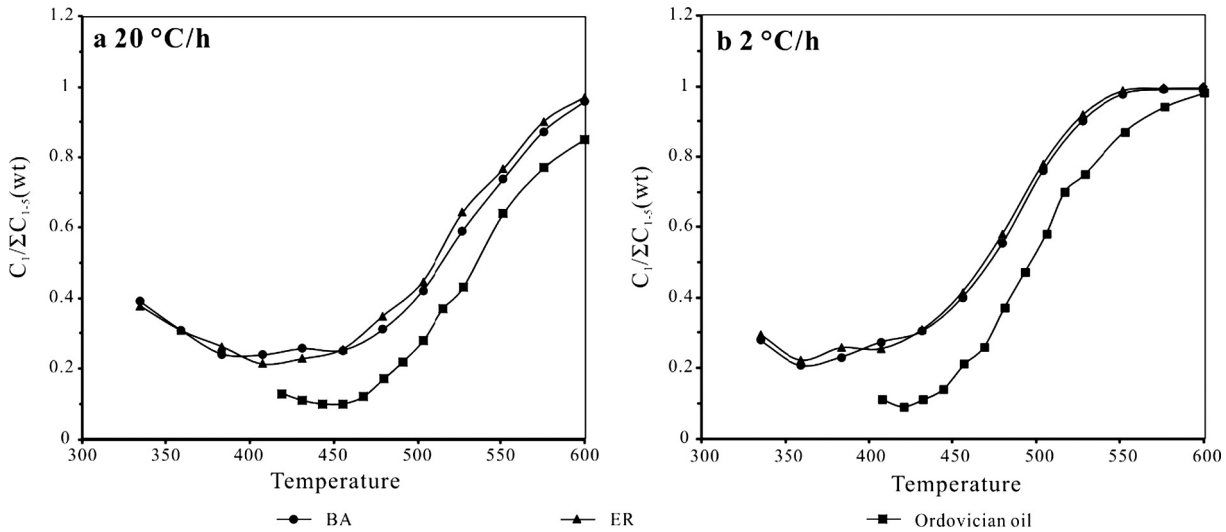

Fig. 3. C_1/C_{1-5} ratio of gaseous hydrocarbons generated by BA and ER pyrolysis experiments versus temperature (data for Ordovician oil are from Pan et al. (2012)).

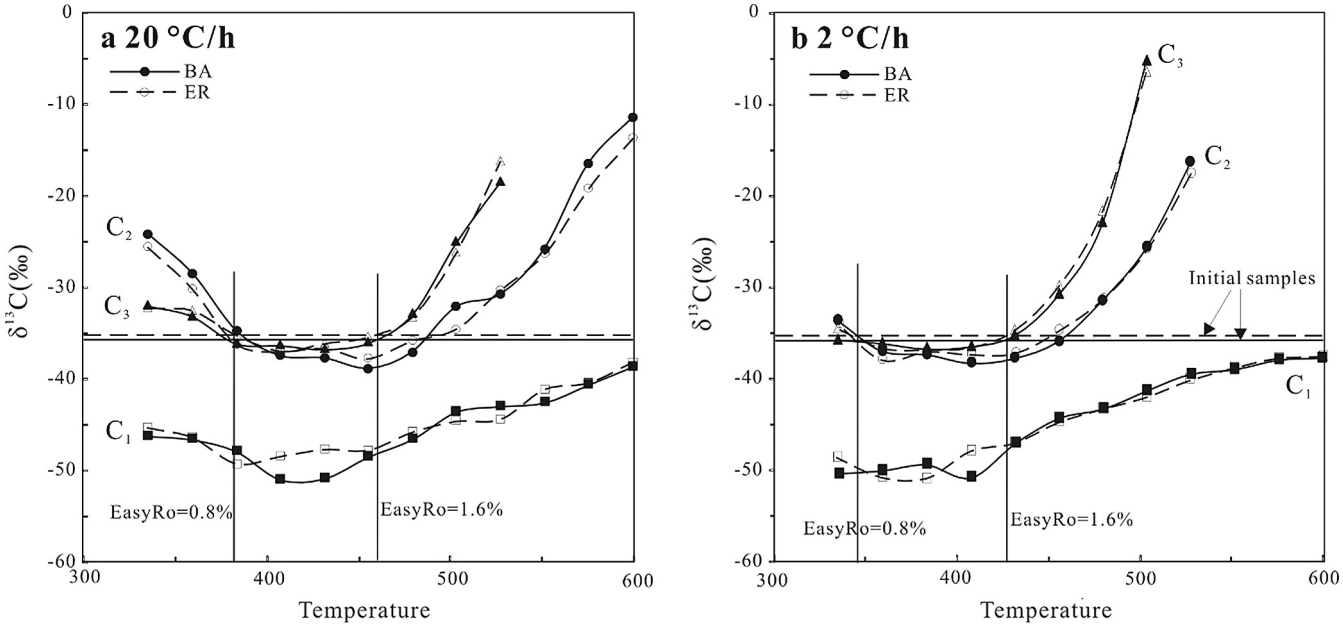

Fig. 4. Stable carbon isotope values for methane, ethane and propane with increasing temperatures at two heating rates of 20 °C/h and 2 °C/h.

significant. The values of $\delta^{13}C_2$ and $\delta^{13}C_3$ are more negative than the bulk carbon isotope values of initial samples (−35.8‰ and −35.2‰ for BA and ER, respectively), but more positive than $\delta^{13}C_1$. (3) When %Ro > 1.6%, $\delta^{13}C_1$, $\delta^{13}C_2$ and $\delta^{13}C_3$ values rapidly increase with maturity. The $\delta^{13}C_1$ values approach and are more negative than the carbon isotope values of the initial BA and ER at all temperatures, and the final $\delta^{13}C$ values of C_1 are similar to those of C_2 and C_3 in stage two. The $\delta^{13}C_2$ and $\delta^{13}C_3$ were higher than the values of initial BA and ER. This is in accord with the Rayleigh Fractionation model.

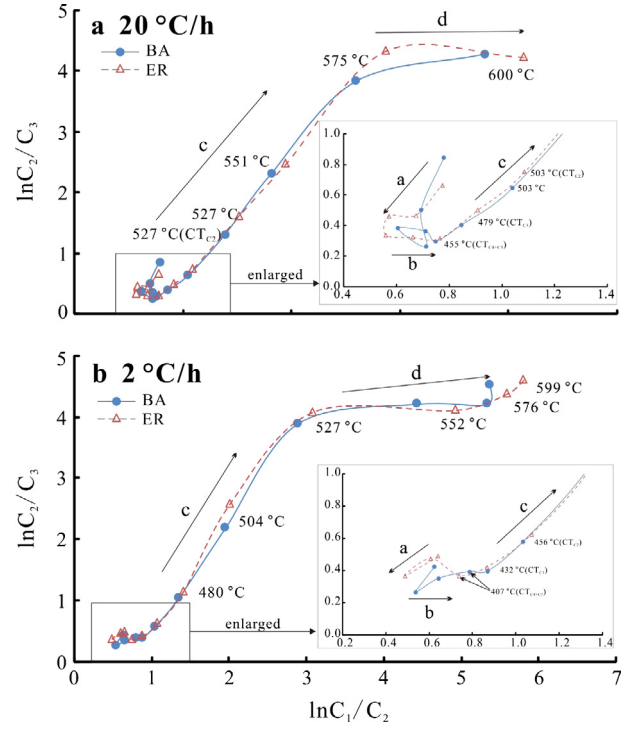

Fig. 5. Plots of $\ln C_1/C_2$ versus $\ln C_2/C_3$ for gases from BA and ER pyrolysis.

3.4. Evolution of hydrocarbon gases during pyrolysis

The pyrolysis experiments are closed-system experiments. Therefore, the analysis of gas composition and the evolution of stable carbon isotope composition in the gas are based on the net yields of generation and decomposition via different pathways.

3.4.1. $\ln C_1/C_2$ versus $\ln C_2/C_3$

The plots of $\ln(C_1/C_2)$ versus $\ln(C_2/C_3)$ based on the C_1–C_3 composition of natural gases at different thermal maturities can help distinguishing whether methane is directly sourced from kerogen or, alternatively, by secondary oil cracking (Prinzhofer and Huc, 1995). The C_2/C_3 ratio is almost constant during primary cracking (it may even decrease), whereas it increases drastically during the secondary cracking of oils. In contrast, the ratio of C_1/C_2 increases progressively during primary cracking and is the almost constant during secondary cracking. Plots of $\ln(C_1/C_2)$ versus $\ln(C_2/C_3)$ obtained from BA and ER under two heating regimes are shown in Fig. 5.

On the basis of the molecular proportions from the pyrolysis of Ordovician kukersite kerogen, which is a known hydrocarbon source rock in the Sinian-lower Palaeozoic strata, Wang et al. (2013) suggested that the plots of $\ln(C_1/C_2)$ versus $\ln(C_2/C_3)$ showed four distinct stages. Hydrocarbon gases from our pyrolysis experiments on both BA and ER show similar trends (Fig. 5): (a) An initial slight decrease in both parameters is observed at pyrolysis temperatures below 407 °C for 20 °C/h and 360 °C for 2 °C/h, due to preferential production of $C_3 > C_2 > C_1$. This indicates that the initial cracking of BA and ER preferentially generate heavier hydrocarbon gases than methane. (b) $\ln(C_1/C_2)$ increased as $\ln(C_2/C_3)$ remained relatively unchanged within the temperature ranges of 407–455 °C for 20 °C/h and 360–407 °C for 2 °C/h. This indicates increased production of methane relative to ethane, but little relative change between ethane and propane generation, typical of kerogen cracking. (c) Both parameters showed a sharp increase during this stage. Critical temperatures CT_{C4+C5}, CT_{C3} and CT_{C2} are reached in the early part of this stage, suggesting that decomposition rates exceed generation rates for $C_4 + C_5$, C_3 and C_2 in turn, typical of secondary oil cracking (Prinzhofer and Huc, 1995). (d) At pyrolysis temperatures above 575 °C for 20 °C/h and 527 °C for

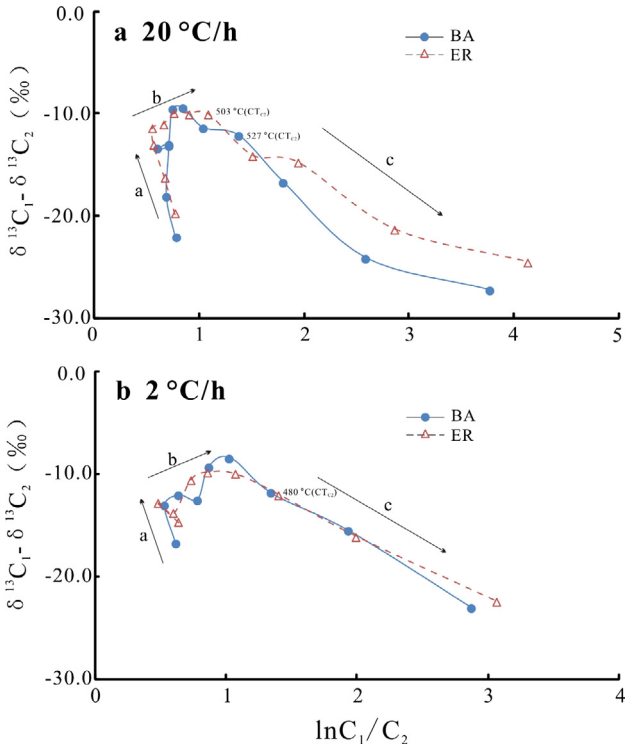

Fig. 6. Plots of $\ln C_1/C_2$ versus $\delta^{13}C_1$–$\delta^{13}C_2$ for gases from BA and ER pyrolysis.

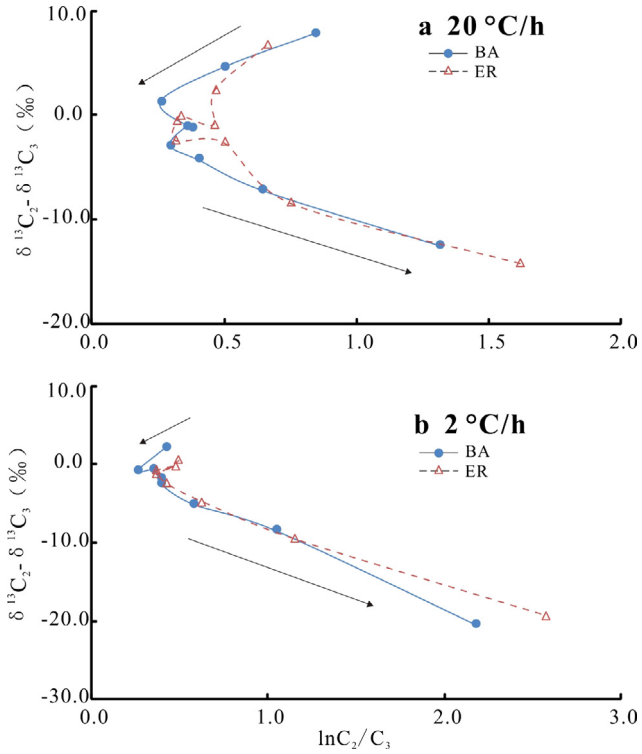

Fig. 7. Plots of $\ln C_2/C_3$ versus $\delta^{13}C_2$–$\delta^{13}C_3$ for gases from BA and ER pyrolysis.

2 °C/h, both of the parameters show trends similar to the second stage but with larger $\ln(C_1/C_2)$ and $\ln(C_2/C_3)$ ratios. Given that almost all of the C_2 is present in the wet gas at this stage, this trend is attributed to the continued cracking of C_2 into C_1 at these very high pyrolysis temperatures.

In addition, during the third stage and the fourth stage, both $\ln(C_1/C_2)$ and $\ln(C_2/C_3)$ are higher for ER than BA at the same temperatures, suggesting that ER generated leaner gases than BA under the same conditions.

3.4.2. $\delta^{13}C_1$–$\delta^{13}C_2$ versus $\ln(C_1/C_2)$

Previous studies have suggested that the plot of $\delta^{13}C_1$–$\delta^{13}C_2$ versus $\ln(C_1/C_2)$ may be useful in elucidating the origins of hydrocarbon gases (Ricchiuto and Schoell, 1988; Jenden et al., 1993; Prinzhofer and Huc, 1995). In general, a series of thermogenic gases from the same source but with different degrees of maturity will show a positive slope. With increasing maturity, the relative proportion of methane increases, and the difference in the isotopic ratio decreases and tends toward zero but the absolute value remains negative (Prinzhofer and Huc, 1995). Fig. 6 presents the data of gases evolved from pyrolysis of BA and ER in this type of plot. As expected, the evolution of hydrocarbon gas shows three distinct stages although the trend is different from that of Prinzhofer and Huc (1995). The three stages we observe in our experiments are as follows:

(a) A slight decrease in $\ln(C_1/C_2)$ and rapid increase in $\delta^{13}C_1$–$\delta^{13}C_2$ due to preferential production of C_2 over C_1. This suggests preferential initial cracking of BA and ER into ethane over methane. (b) Both parameters show an increase in the second stage, which is similar to the results of Prinzhofer and Huc (1995). This indicates increased production of methane compared with ethane, and the difference between $\delta^{13}C_1$ and $\delta^{13}C_2$ decreases to a minimum. The cracking rates of $C_4 + C_5$, C_3 and C_2 to dry gas successively overtake their generation rates in the later parts of this stage. (c) The data show a rapid decrease in $\delta^{13}C_1$–$\delta^{13}C_2$ values with increasing $\ln(C_1/C_2)$ during the third stage. In this stage, mass yields of total gaseous hydrocarbons (C_{1-5}) do not change appreciably, but methane increases while wet gas components decrease substantially (Table 3). This suggests that methane is generated in this stage mainly by cracking of wet gas components (C_2, C_3, C_4, C_5). Wet gas cracking is characterized by a rapid increase of the $\delta^{13}C$

Table 4
Kinetic parameters for hydrocarbon gases.

Ea (kcal/mol)	C_1 (%) 1×10^{14} S^{-1}		C_{1-5} (%) 1×10^{15} S^{-1}	
	BA	ER	BA	ER
51	0.42	0.10		
52	0.39	1.30		
53	0.00	0.54	0.16	0.00
54	2.77	0.00	1.36	1.29
55	0.00	3.93	0.00	1.76
56	4.74	1.40	2.59	0.58
57	0.00	0.00	4.04	5.28
58	5.81	10.33	0.00	0.00
59	6.67	0.00	10.51	10.69
60	0.00	8.37	0.00	0.00
61	11.26	10.78	9.22	11.94
62	5.51	0.00	14.61	11.26
63	5.61	15.63	0.00	0.00
64	10.31	1.45	12.37	20.57
65	16.23	14.18	8.82	0.00
66	0.00	13.52	0.00	3.59
67	13.82	0.00	7.73	11.16
68	0.00	15.36	10.30	0.00
69	9.97	0.00	3.42	5.00
70	5.19	0.00	0.00	13.24
71	0.00	0.73	8.60	0.00
72	0.00	0.86	0.00	1.71
73	1.31	0.85	0.00	0.00
74	0.00	0.68	4.26	0.00
75			0.76	0.00
76			0.00	0.00
77			1.25	0.00

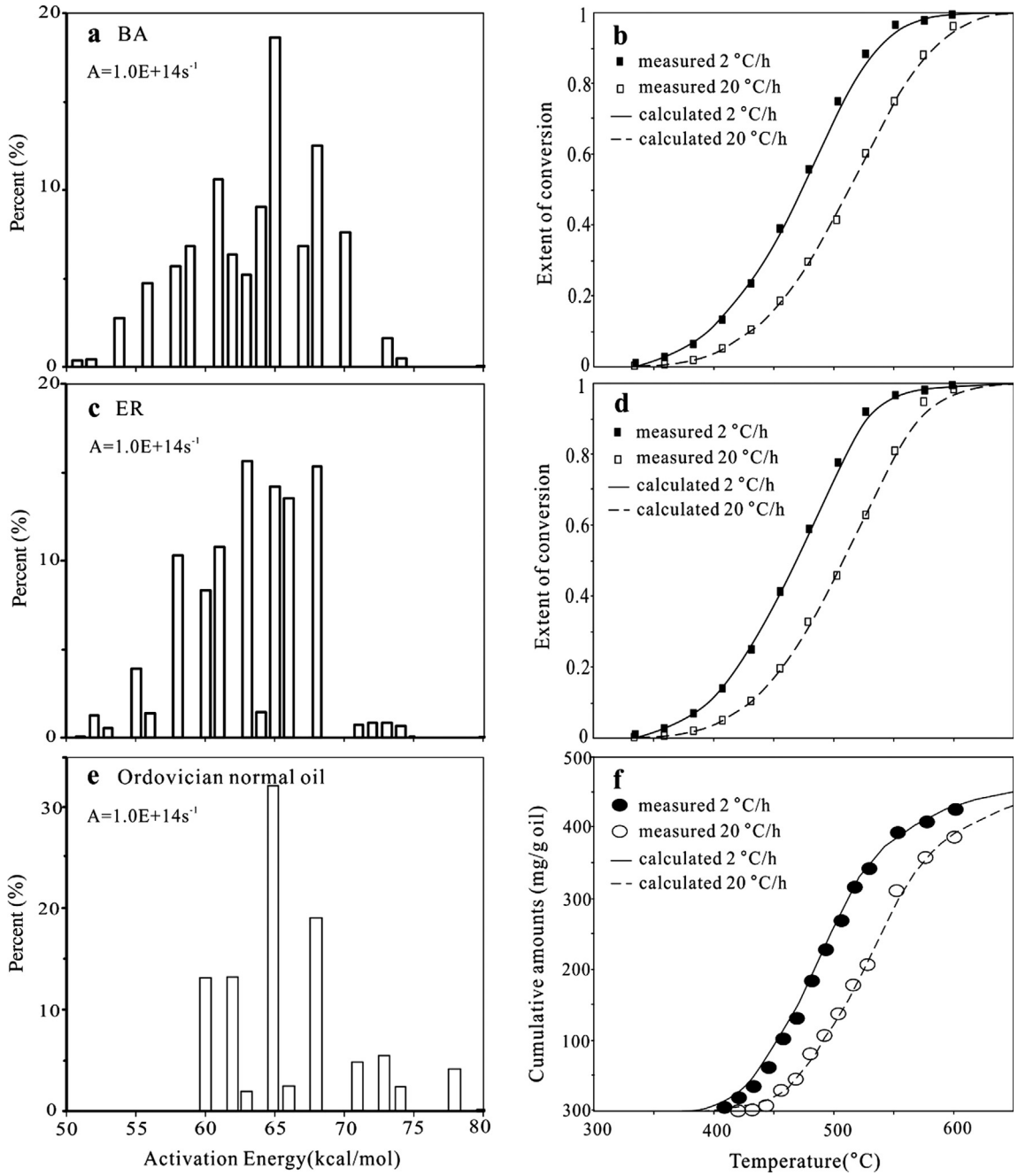

Fig. 8. Activation energy distributions using frequency factor $1 \times 10^{14}\,S^{-1}$ for methane generation from BA, ER and Ordovician normal oil, and the conversion of methane compared with measured results (data of Ordovician normal oil are from Pan et al. (2012)).

value of ethane and a relatively slow increase of the $\delta^{13}C$ value of methane, leading to the rapid increase in the difference between the $\delta^{13}C$ values of ethane and methane.

Based on our observations, we conclude that the trends proposed by Prinzhofer and Huc (1995) only represents part of the three stages we observed.

3.4.3. $\delta^{13}C_2$–$\delta^{13}C_3$ versus ln(C_2/C_3)

Prinzhofer and Huc (1995) also proposed an evolutionary model for both oil cracking and kerogen maturation using the plot of $\delta^{13}C_2$–$\delta^{13}C_3$ versus ln(C_2/C_3). Plots of this model have been widely applied to identify the two gas types in the petroleum bearing basins in China with high thermal maturation levels (Chang et al., 2001; Qin et al., 2005; Zhang et al., 2007). However, the trends of hydrocarbon gases generated from our experiments on pyrolysis of BA and ER are very different from what has been previously reported. As illustrated in Fig. 7, $\delta^{13}C_2$–$\delta^{13}C_3$, which is initially greater than zero, trends toward zero with decreasing ln (C_2/C_3) (i.e., increasing thermal stress and primary cracking of kerogen). Both parameters remain relatively constant in the stage of secondary oil cracking. Finally, in the wet gas cracking stage, the data shows a rapid decrease in $\delta^{13}C_2$–$\delta^{13}C_3$ values with increasing ln(C_2/C_3), similar to stage (c) in the plot of $\delta^{13}C_1$–$\delta^{13}C_2$ versus ln (C_1/C_2). Guo et al. (2009) have suggested that $\delta^{13}C_2$–$\delta^{13}C_3$ of the

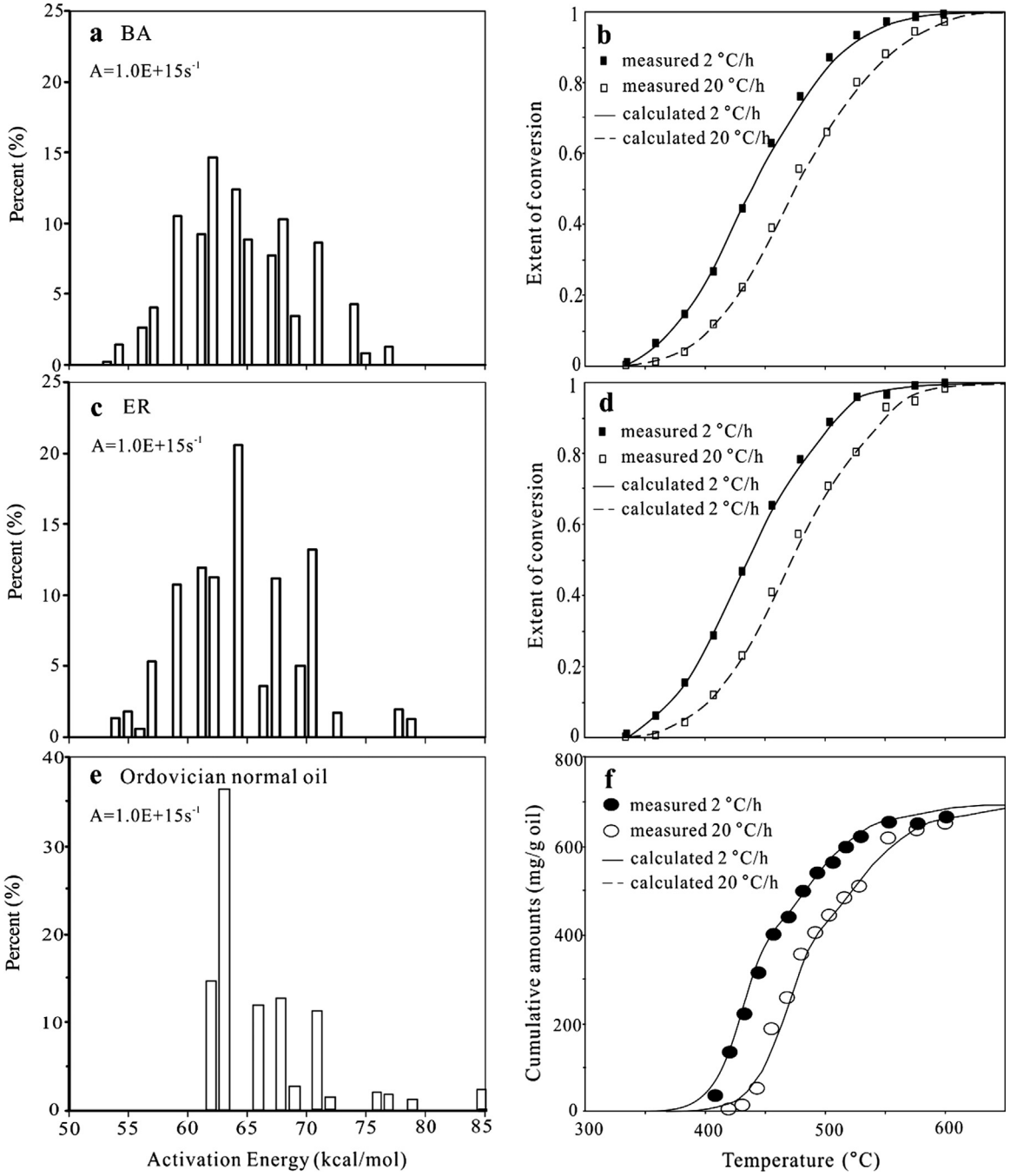

Fig. 9. Activation energy distribution with the frequency factor $1 \times 10^{15}\ S^{-1}$ of total gaseous hydrocarbons generation from BA, ER and Ordovician normal oil, and the conversion of C_{1-5} compared with measured results (data of Ordovician normal oil are from Pan et al. (2012)).

oil-derived gases increases rapidly, while that of kerogen-derived gases has only a slight increase with increasing $\ln(C_2/C_3)$ value (i.e., increasing thermal stress).

3.5. Kinetic parameter

3.5.1. Kinetic parameters for the generation of methane and total hydrocarbon gases

Methane and total hydrocarbon gases formed at the different heating rates in our experiments all reach a plateau in cumulative yields which we believe indicates that they have basically reached the end of generation. As a consequence, these data can serve as direct input for the calculation of kinetic parameters. Hydrocarbon gas generation from kerogen and oil cracking is generally described using simple first-order kinetics with a single frequency factor (A) and a distribution of activation energies (Ea) (Ungerer and Pelet, 1987; Schenk and Horsfield, 1993; Tang et al., 1996; Behar et al., 1997; Dieckmann et al., 2002, 2006; Dieckmann, 2005). Several previous studies have documented the compensation effect between the frequency factor (A) and the activation energies, and suggested a universal frequency factor for the kinetics of oil generation and destruction (Pelet, 1994; Waples, 2000; Pan et al., 2010, 2012). Pan et al. (2010, 2012) suggested universal frequency factors of $1 \times 10^{14}\ S^{-1}$ and $1 \times 10^{15}\ S^{-1}$ for methane and total hydrocarbon gases generation, respectively. To avoid the compensation effects and to be able to compare with previous studies, we

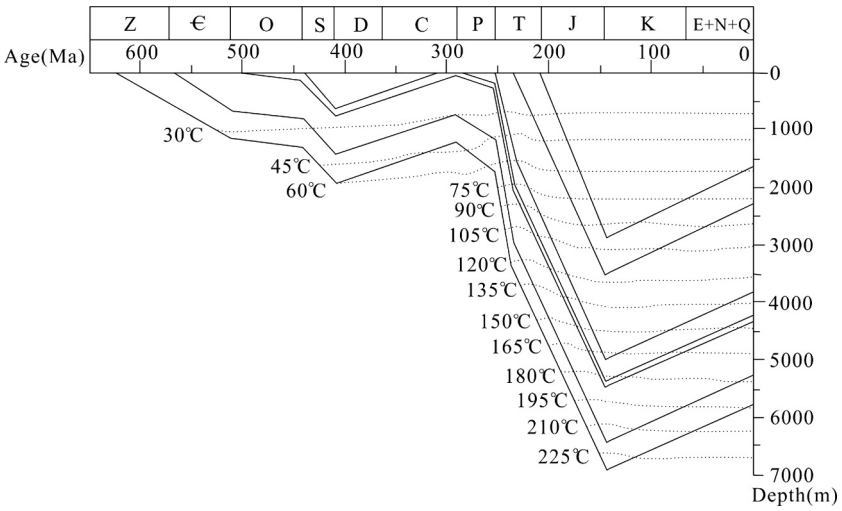

Fig. 10. Burial history of Well Gaoke-1 from the central Sichuan Basin.

used these fixed frequency factors of Pan et al. (2010, 2012) for both sets of experiments. The kinetic parameters for the generation of methane and total hydrocarbon gases are listed in Table 4. The Ea distributions and the fit of the conversion values calculated from the kinetic parameters and measured from the experimental data for methane and total hydrocarbon gases are shown in Figs. 8 and 9.

The Ea of the methane and total hydrocarbon gases generated from the BA and ER exhibit similar distribution patterns, varying from 51 to 75 kcal/mol with $A = 1 \times 10^{14}\ S^{-1}$ for methane generation and 54 to 78 kcal/mol with $A = 1 \times 10^{15}\ S^{-1}$ for total hydrocarbon gases generation. The component and stable carbon isotopes of hydrocarbon gases for BA and ER show almost the same evolutionary characteristics.

As with the Ordovician oil studied by Pan et al. (2010, 2012), the predominant Ea of methane generated from BA is 65 kcal/mol with a fixed A factor $1 \times 10^{14}\ S^{-1}$. However, the Ea distribution of methane generated from our experiments using BA is in the range 51–75 kcal/mol and is far lower than that of Ordovician oil (i.e., 60–78 kcal/mol). This indicates that more methane is generated from BA at Ea < 60 kcal/mol and could be attributed to the differences in gross composition (SARA) of the Ordovician oil compared to BA. The Ordovician oil used by Pan et al. (2010, 2012) is rich in saturates (81.7%), while BA is predominantly made up of asphaltenes (83.9%). This is in line with previous studies which have suggested that hydrocarbon gas generation potential is higher for asphaltenes than saturates in the early stages of thermal evolution (Tian et al., 2012).

In addition, the Ea distributions of total hydrocarbon gases generation from BA and ER are relatively more smooth and Gaussian than those from the Ordovician oil. Fig. 9d–f shows that the total hydrocarbon gas generation curves for BA and ER are relatively gentler, while they are steeper for the Ordovician oil. This may indicate that hydrocarbon gas generation from asphaltenes are more gradual and continuous compared with a very rapid onset and initial high yield for generation from saturates.

3.6. Extrapolation to geological conditions

We applied the compositional kinetic model derived from our results to the burial history of the basin as represented by the geological profile of well Gaoke-1, located in the Gaoshiti-Moxi gasfield. The Gaoshiti-Moxi is the largest integral marine gas reservoir in China (Zou et al., 2014) and the area it is located in has

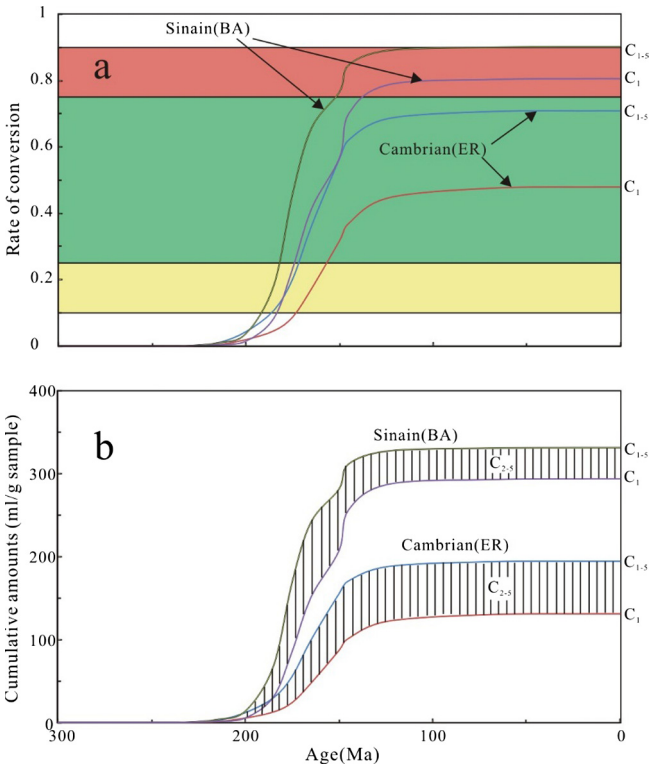

Fig. 11. Hydrocarbon gas generation history for Cambrian and Sinian bitumen.

experienced two episodes of sedimentation and uplift during its tectonic evolution, controlled by the Caledonian and Himalayan orogenies. For our simulations, we used the burial history of Well Gaoke-1 as modelled by Zhang et al. (2007) (Fig. 10). The geological history indicates that the Caledonian orogeny locally lasted from the end of Silurian to the beginning of Permian, resulting in the absence of Devonian and Carboniferous strata and the erosion of Upper Silurian strata. The area continued to receive sediments from the Early Permian to the Early Cretaceous, with the development of a thick Mesozoic section. Strong uplift began at the end of the Early Cretaceous in this area, resulting in the total erosion of the Lower Cretaceous, Jurassic and part of the Upper Triassic strata. The present burial depths of the Sinian and Lower

Table 5
Geochemical parameters of the Sinian-Cambrian gases in the Gaoshiti-Moxi area of the Sichuan Basin.[a]

Wells	Strata	Hydrocarbon gas composition (%)			$(C_2 + C_3)/C_1 * 100$ (%)	Isotopes (‰)	
		C_1	C_2	C_3		$\delta^{13}C_1$	$\delta^{13}C_2$
Gaoshi-1	Z_2d^{4-2}	91.19	0.09	0.001	0.100	−32.2	−28.2
Gaoshi-1	Z_2d^{4-1}	90.12	0.04	0.002	0.047	−32.6	−28.5
Gaoshi-1	Z_2d^{2}	82.66	0.04	0.001	0.050	−32.2	−28.8
Gaoshi-3	Z_2d^{4-2}	90.18	0.04	0.001	0.045	−33.2	−28.2
Gaoshi-6	Z_2d^{4-1}	89.97	0.04	0.001	0.046	−32.8	−28.7
Gaoshi-6	Z_2d^{2}	94.6	0.05	0.002	0.055	−32.8	−29.1
Moxi-8	Z_2d^{2}	91.41	0.03	0.001	0.034	−32.8	−28.3
Moxi-8	Z_2d^{1}	91.43	0.04	0.001	0.045	−32.3	−27.5
Moxi-9	Z_2d^{2}	91.81	0.05	0.001	0.056	−33.4	−28.7
Moxi-10	Z_2d^{2}	93.12	0.05	0.002	0.056	−33.9	−27.8
Moxi-11	Z_2d^{2}	89.88	0.03	0.001	0.034 0.051[b]	−32.1	−26.9
Moxi-8	ϵ_1L^{2}	96.81	0.14	0.009	0.154	−32.5	−32.4
Moxi-8	ϵ_1L^{1}	96.84	0.14	0.01	0.155	−33.2	−33.7
Moxi-9	ϵ_1L	95.15	0.13	0.007	0.144	−32.9	−32.8
Moxi-11	ϵ_1L^{2}	97.08	0.13	0.005	0.139	−32.5	−32.4
Moxi-11	ϵ_1L^{1}	97.11	0.13	0.004	0.138 0.146[c]	−32.6	−32.5

[a] Data are from Zou et al. (2014).
[b] Average in Sinian.
[c] Average in Cambrian.

Cambrian are approximately 5750 and 4986 m, respectively. The Sinian-Cambrian strata form an important petroleum system in this area, but the source of the natural gas in the Sinian-Cambrian reservoirs is still not resolved (Zou et al., 2014). Abundant pyrobitumen is found in the Sinian–Cambrian strata in Well Gaoke-1 and previous studies have proposed that this is derived from crude oil generated by Cambrian black shales and charged into the Sinian strata in the early middle Jurassic (Zhang et al., 2005; Xu et al., 2007a, 2007b). This crude oil has been proposed as a significant secondary hydrocarbon (gas) source in the Sinian. However, the precise nature of this crude oil is unknown.

In this paper, we assume that BA and ER were a significant secondary hydrocarbon sources in Sinian and Cambrian strata, i.e., ER is the Cambrian residual organic matter and BA is the Sinian reservoired crude oil. Then we modelled these with the kinetic parameters derived from our experiments using the burial history determined from Well Gaoke-1. The results of the modelled gas generation history are shown in Fig. 11.

According to the model, hydrocarbon gas generation from ER started in the Middle Jurassic (approximately 175 Ma), and ended in the Early Cretaceous (approximately 125 Ma) due to inversion after achieving a maximum maturity equivalent to Easy%Ro of ≈2.2%. The final conversion of C_{1-5} and C_1 are 0.71 and 0.48, respectively, and the final wetness (C_{2-5}/C_{1-5}) is 32.6%. Hydrocarbon gas generation from BA started in the Early Jurassic (approximately 185 Ma), and ended in the Early Cretaceous (approximately 125 Ma) with a final maturity of around Easy%Ro ≈ 3.0%. The final conversion of C_{1-5} and C_1 are 0.90 and 0.81, respectively, and the final C_{2-5}/C_{1-5} is 11.3%.

The model results indicate that the conversion of C_{1-5} and C_1 are higher for Sinian reservoired crude oil than for Cambrian residual organic matter, and the wetness of the final hydrocarbon gas is lower from Sinian reservoired crude oil than from Cambrian residual organic matter. This is partly attributed to the higher maturity of the Sinian than the Cambrian. Supporting these results is the observation that the wetness of produced natural gas is lower in Sinian reservoirs than Cambrian ones in the Gaoshiti-Moxi area (Table 5).

Both sets of experimentally generated hydrocarbon gases have higher wetnesses than corresponding produced natural gases. This is probably due to the closed system nature of the experiments, compared to the more open geological conditions of the natural systems. In summary, our results suggest that Sinian reservoired natural gases were generated from Sinian reservoired crude oil, and Cambrian reservoired natural gases originated from Cambrian residual organic matter.

4. Conclusions

Two sets of pyrolysis experiments were performed for BA and ER of low-maturity bitumen at two heating rates of 2 °C/h and 20 °C/h in confined systems. Kinetic parameters derived from BA and ER were applied to simulate hydrocarbon generation from Cambrian and Sinian strata. The main observations are:

(1) BA and ER have high hydrocarbon generation and exhibit similar evolutionary characteristics of gas generation.
(2) Hydrocarbon gas generation from BA and ER have higher C_1/C_{1-5} values than those from pyrolysis of Ordovician normal oil. The Ea distribution of methane generation from BA and ER is far lower than that of the Ordovician normal oil.
(3) The evolution of stable carbon isotope values of individual hydrocarbon gases may be divided into three stages. Plots of $\ln C_1/C_2$ versus $\ln C_2/C_3$, $\delta^{13}C_1-\delta^{13}C_2$ versus $\ln(C_1/C_2)$ and $\delta^{13}C_2-\delta^{13}C_3$ versus $\ln(C_2/C_3)$ are useful in illustrating this process and characteristics of hydrocarbon gases from BA and ER through the different maturity stages.
(4) Model results indicate that hydrocarbon gas generation from ER started in the Middle Jurassic, and ended in the Early Cretaceous with achieving a maturity equivalent of Easy% Ro ≈ 2.2%. The final conversion rate of C_{1-5} and C_1 are 0.71 and 0.48, respectively. Hydrocarbon gas generation from BA started in the Early Jurassic, and ended in the Early Cretaceous with an equivalent Easy%Ro ≈ 3.0%. The final conversion rate of C_{1-5} and C_1 are 0.90 and 0.81, respectively.

Acknowledgments

This research was supported by the Chinese Academic of Sciences Key Project (Grant No. XDB10030404) and the National Programs for Fundamental Research and Development of China

(973 Program) (Grant No. 2012CB214700), the Chinese Academic of Sciences Key Project (Grant No. XDB03020405), the National Natural Science Foundation of China (Grant Nos. 41572350, 41172169, 41272147 and 40672123), Western Light Joint Scholars Project and the Key Laboratory Project of Gansu Province (Grant No. 1309RTSA041).

Special thanks go to anonymous reviewers, Associate Editor Dariusz Strapoc and Editor-in-Chief Erdem Idiz for their efforts on this paper.

Associate Editor—**Darius Strapoc**

References

Behar, F., Vandenbroucke, M., Tang, Y., Marquis, F., Espitalie, J., 1997. Thermal cracking of kerogen in open and closed systems: determination of kinetic parameters and stoichiometric coefficients for oil and gas generation. Organic Geochemistry 26, 321–339.

Braun, R.L., Burnham, A.K., 1998. Kinetics GUI.exe, Version 1.11.

Chang, Y.H., Wang, T.D., Wang, S.Y., Lin, F., 2001. Differences between kerogen and oil cracked gases in Sinian reservoirs of Weiyuan and Ziyang area. Acta Sedimentologica Sinica 19 (1), 156–160.

Deng, H.C., Zhou, W., Zhou, Q.D., Xie, R.C., 2008. Oil sand-forming conditions and evaluation on resource of oil sand in Tianjingshan structure in northwest part of Sichuan Basin. Journal of Jilin University (Earth Science Edition) 38, 69–75.

Dieckmann, V., 2005. Modelling petroleum formation from heterogeneous source rocks: the influence of frequency factors on activation energy distribution and geological prediction. Marine and Petroleum Geology 22, 375–390.

Dieckmann, V., Caccialanzaa, P.G., Galimbertia, R., 2002. Evaluating the timing of oil expulsion: about the inverse behaviour of light hydrocarbons and oil asphaltene kinetics. Organic Geochemistry 33, 1501–1513.

Dieckmann, V., Ondrak, R., Cramer, B., Horsfield, B., 2006. Deep basin gas: new insights from kinetic modelling and isotopic fractionation in deep-formed gas precursors. Marine and Petroleum Geology 23, 183–199.

Du, J.H., Zou, C.N., Xu, C.C., He, H.Q., Sheng, P., Yang, Y.M., Li, Y.L., Wei, G.Q., Wang, Z. C., Yang, Y., 2014. Theoretical and technical innovations in strategic discovery of a giant gas field in Cambrian Longwangmiao Formation of central Sichuan paleo-uplift, Sichuan Basin. Petroleum Exploration & Development 41, 294–305.

Guo, L.G., Xiao, X.M., Tian, H., Song, Z.G., 2009. Distinguishing gases derived from oil cracking and kerogen maturation: insights from laboratory pyrolysis experiments. Organic Geochemistry 40 (10), 1074–1084.

Huang, D.F., Wang, L.S., 2008. Geochemical characteristics of bituminous dike in Kuangshanliang area of the Northwestern Sichuan Basin and its significance. Acta Petrolei Sinica 29, 23–28.

Jenden, P.D., Drazan, D.J., Kaplan, I.R., 1993. Mixing of thermogenic natural gases in Northern Appalachian Basin. American Association of Petroleum Geologists Bulletin 77, 980–998.

Jin, X.D., Pan, C.C., Yu, S., Li, E.T., Wang, J., Fu, X.D., Qin, J.Z., Xie, Z.Y., Zheng, P., Wang, L.S., Chen, J.P., Tan, Y.M., 2014. Organic geochemistry of marine source rocks and pyrobitumen-containing reservoir rocks of the Sichuan Basin and neighbouring areas, SW China. Marine and Petroleum Geology 56, 147–165.

Liu, D.L., Dai, J.X., Xiao, X.M., Tian, H., Yang, C., Hu, A.P., Mi, J.K., Song, Z.G., 2009. High density methane inclusions in Puguang Gasfield: discovery and a T-P genetic study. Chinese Science Bulletin 54, 4714–4723.

Pan, C., Geng, A., Zhong, N., Liu, J., Yu, L., 2008. Kerogen pyrolysis in the presence and absence of water and minerals. Part 1. Gas components. Energy & Fuels 22, 416–427.

Pan, C., Jiang, L., Liu, J., Zhang, S., Zhu, G., 2010. The effects of calcite and montmorillonite on oil cracking in confined pyrolysis experiments. Organic Geochemistry 41, 611–626.

Pan, C., Jiang, L., Liu, J., Zhang, S., Zhu, G., 2012. The effects of pyrobitumen on oil cracking in confined pyrolysis experiments. Organic Geochemistry 45, 29–47.

Pan, C., Yu, L., Liu, J., Fu, J., 2006. Chemical and carbon isotopic fractionations of gaseous hydrocarbons during abiogenic oxidation. Earth and Planetary Science Letters 246, 70–89.

Pelet, R., 1994. Comments on the paper "The effects of the mineral matrix on the determination of kinetic parameters using modified Rock-Eval pyrolysis" by H. Dembicki Jr., Organic Geochemistry, 18, 531–539 (1992). Organic Geochemistry 21, 979–981.

Prinzhofer, A.A., Huc, A.Y., 1995. Genetic and post-genetic molecular and isotopic fractionations in natural gases. Chemical Geology 126 (95), 281–290.

Qin, S.F., Li, M., Dai, J.X.D., Xiao, Z.Y., Zhang, Q.C., 2005. Types of cracking gas in Hetianhe gas field in Tarim basin. Oil and Gas Geology 26 (4), 455–460.

Ricchiuto, T., Schoell, M., 1988. Origin of natural gases in the Apulian Basin in south Italy: a case history of mixing of gases of deep and shallow origin. Organic Geochemistry 13, 311–318.

Schenk, H.J., Horsfield, B., 1993. Kinetics of petroleum generation by programmed temperature closed- versus open-system pyrolysis. Geochimica et Cosmochimica Acta 57, 623–630.

Sweeney, J.J., Burnham, A.K., 1990. Evaluation of a simple model of vitrinite reflectance based on chemical-kinetics. American Association of Petroleum Geologists Bulletin 74, 1559–1570.

Tang, Y., Jenden, P.D., Nigrini, A., Teerman, S.C., 1996. Modeling early methane generation in coal. Energy & Fuels 10, 659–671.

Tian, H., Xiao, X., Wilkins, R.W.T., Tang, Y., 2012. An experimental comparison of gas generation from three oil fractions: implications for the chemical and stable carbon isotopic signatures of oil cracking gas. Organic Geochemistry 46, 96–112.

Ungerer, P., Pelet, R., 1987. Extrapolation of the kinetics of oil and gas formation from laboratory experiments to sedimentary basins. Nature 327, 52–54.

Wang, Q.T., Lu, H., Greenwood, P., Shen, C.C., Liu, J.Z., Peng, P.A., 2013. Gas evolution during pyrolysis of Estonian Kukersite shale in confined gold tube system. Organic Geochemistry 65, 74–82.

Wang, T.S., Geng, A.S., Li, X., Xu, Z.H., 2010. Gas-Generation mechanism of the pyrolysis of asphaltenes in marine crude oil and its geological application. Acta Sedimentological Sinica 28, 808–814.

Waples, D.W., 2000. The kinetics of in-reservoir oil destruction and gas formation: constraints from experimental and empirical data, and from thermodynamics. Organic Geochemistry 31, 553–575.

Wei, S., Liu, S.G.M.Y., Cai, X.Y., Xu, G.S., Wang, G.Z., Yong, Z.Q., Yuan, H.F., Pan, C.L., 2007. Determination and quantitative simulation of gas pool formation process of Sinian cracked aas in Weiyuan—Ziyang area, Sichuan Basin. Acta Geologica Sinica 81, 1153–1159.

Xiao, X.M., Wang, F., Wilkins, R.W.T., Song, Z.G., 2007. Origin and gas potential of pyrobitumen in the Upper Proterozoic strata from the Middle Paleo-Uplift of the Sichuan Basin, China. International Journal of Coal Geology 70, 264–276.

Xie, Z.Y., Tian, S.C., Wei, G.Q., Li, J., Zhang, L., Yang, W., 2005. The study on bitumen and foregone pool of Feixiguanoolitic in northeast Sichuang Basin. Natural Gas Geoscience 16, 283–288.

Xu, G.S., Xu, Y.L., Yuan, H.F., Ma, Y.S., Cai, X.Y., Cui, J.W., 2007a. Geochemical characteristics of source rocks and reservoir bitumen of Sinian-Lower Palaeozoic in the middle-southwest of Sichuan Basin. Journal of Oil and Gas Technology 29 (4), 45–51.

Xu, G.S., Yuan, H.F., Ma, Y.S., Liu, S.G., Cai, X.Y., Wang, G.Z., Pan, C.L., 2007b. The source of Sinian and Lower-Palaeozoic bitumen and hydrocarbon evolution in the middle and southeast of the Sichuan Basin. Acta Geologica Sinica 81, 1143–1152.

Zhang, L., Wei, G.Q., Li, X.Z., Wang, Z.C., Xiao, X.M., 2007. The thermal history of Sinian-Lower Palaeozic high/over mature source rock in Sichuan Basin. Natural Gas Geoscience 18 (5), 726–731.

Zhang, L., Wei, G.Q., Wu, S.X., Wang, Z.C., Xiao, X.M., Zhang, P.J., Sheng, J.H., 2005. Distribution characters and hydrocarbon-generation potential of bitumen of Sinian-Lower Paleozoic in Sichuan Basin. Petroleum Geology & Experiment 27, 276–280 + 298.

Zhang, S.C., Zhu, G.Y., Chen, J.P., Liang, Y.B., 2007. A discussion on gas sources of the Feixiansuan Formation H_2S-rich giant gas fields in the northeastern Sichuan Basin. Chinese Science Bulletin 52 (1), 113–124.

Zhang, Z.R., Hu, W.X., Song, X.Y., Zhang, C.M., Zhang, Q., Jin, J.C., 2014. A comparison of results from two different flash pyrolysis methods on a solid bitumen sample. Organic Geochemistry 69, 36–41.

Zhou, Q., Xiao, X.M., Tian, H., Wilkins, R.W.T., 2013. Oil charge history of bitumens of differing maturities in exhumed Palaeozoic reservoir rocks at Tianjingshan, NW Sichuan Basin, Southern, China. Journal of Petroleum Geology 36, 363–382.

Zhou, W., Deng, H.C., Qiu, D.Z., Xie, R.C., 2007. The discovery and significance of the Devonian paleo-reservoir in Tianjingshan structure of the Northwest Sichuan, China. Journal of Chengdu University of Technology (Science & Technology Edition) 34, 413–417.

Zou, C.N., Wei, G.Q., Xu, C.C., Du, J.H., Xie, Z.Y., Wang, Z.C., Hou, L.H., Yang, C., Li, J., Yang, W., 2014. Geochemistry of the Sinian-Cambrian gas system in the Sichuan Basin, China. Organic Geochemistry 74, 13–21.